The cytoplasmic incompatibility Cif proteins from prophage WO modify sperm genome integrity

Short title: The cytoplasmic incompatibility proteins modify sperm genome integrity

Authors: Rupinder Kaur[1,2,*], Brittany A. Leigh[1,2,*], Isabella T. Ritchie[1,2] and Seth R. Bordenstein[1,2,3,4,5]

Affiliations:

[1] Vanderbilt University, Department of Biological Sciences, Nashville, TN, USA

[2] Vanderbilt University, Vanderbilt Microbiome Innovation Center, Nashville, TN, USA

[3] Vanderbilt University Medical Center, Department of Pathology, Microbiology & Immunology, Nashville, TN, USA

[4] Vanderbilt University Medical Center, Vanderbilt Institute for Infection, Immunology and Inflammation, Nashville, TN, USA

[*] Co-first authors

[5] Correspondence to:

Seth R. Bordenstein, Nashville, TN, 37235, Phone 615.322.9087, e-mail s.bordenstein@vanderbilt.edu

Abstract

Inherited microorganisms can selfishly manipulate host reproduction to drive through populations. In *Drosophila melanogaster*, germline expression of the native prophage WO proteins CifA and CifB cause cytoplasmic incompatibility (CI) in which sperms fertilize uninfected embryos that suffer catastrophic mitotic defects and lethality; however in infected females, CifA rescues the embryonic lethality and thus imparts a fitness advantage to *Wolbachia*. Despite widespread relevance to sex determination, evolution, and vector control, the mechanisms underlying when and how CI impairs male reproduction remain unknown and a topic of debate. Here we use cytochemical, microscopic, and transgenic assays in *D. melanogaster* to demonstrate that CifA and CifB proteins of *w*Mel localize to nuclear DNA throughout the process of spermatogenesis. Cif proteins cause abnormal histone retention in elongating spermatids and protamine deficiency in mature sperms of CI-causing males. Protamine-deficient sperms travel to the female reproductive tract together with Cif proteins. In female ovaries, CifA localizes to germ cell nuclei and overlaps with *Wolbachia* in the nurse cell cytoplasm and the oocyte, however Cifs are not present in late-stage oocytes and the embryo. Moreover, CI and rescue are contingent upon a newly annotated CifA bipartite nuclear localization sequence. Our results reveal a previously unrecognized phenomena in which prophage proteins invade animal gametic nuclei and modify the histone-protamine transition of spermatogenesis.

Introduction

Numerous animal species harbor heritable microorganisms that alter host fitness in beneficial and harmful ways. The most common, maternally-inherited bacteria are *Wolbachia*, and they typically reside intracellularly in reproductive tissues of both male and female arthropods. Here, they induce reproductive modifications with sex specific effects such as cytoplasmic incompatibility (CI) that can rapidly drive the bacteria to high frequencies in host populations. CI also notably yields important consequences on arthropod speciation [1–3] and vector control strategies [4–9] by causing lethality of embryos from *Wolbachia*-infected males and uninfected females. As CI is rescued by *Wolbachia*-infected females with the same strain [10,11], the phenotype accordingly imparts a relative fitness advantage to infected females that transmit the bacteria [12].

Two genes, *cytoplasmic incompatibility factors cifA* and *cifB*, occur in a *Wolbachia* prophage WO module enriched with predicted arthropod functions and homology [13–15]. We previously demonstrated that dual, transgenic expression of *cifA* and *cifB* from *w*Mel *Wolbachia* in *Drosophila melanogaster* males can induce CI, while single expression of *cifA* in females rescues CI [16,17]. These results form the basis of the Two-by-One genetic model of CI for several, but not all, strains of *Wolbachia* [13,15,18,19]. At the cellular level, CI-defining lethality associates with chromatin defects and mitotic arrest within the first few hours of embryonic development. Normally after fertilization, the sperm-bound proteins ‘protamines’ are removed in the embryo and replaced by maternally supplied ‘histones’, resulting in the rapid remodeling of the paternal chromatin [20]. However, during CI, there is a delay in the deposition of maternal histones onto the paternal chromatin, resulting in altered DNA replication, failed chromosome condensation, and various mitotic defects that generate embryonic death [13,21–27].

The incipient, pre-fertilization events in the reproductive tissues that establish CI and rescue remain enigmatic and under recent debate, namely whether (i) the Cifs establish CI during spermatogenesis (Host-Modification model) or embryogenesis (Toxin-Antidote model) and whether rescue occurs or does not occur by CifA and CifB binding in the embryo [28,29]. Here, we develop antibodies to localize Cif proteins from *w*Mel *Wolbachia* during *D. melanogaster* gametogenesis and embryogenesis and perform genome integrity measurements of developing sperm across transgenic, mutant, and wild type treatment groups. We describe the following cell biological and gametic chromatin events underpinning CI: (i) CifA and CifB proteins localize to the developing sperm nuclei from early spermatogonium stage to late elongating spermatids; (ii) In mature sperm, CifA associates with sperm tails and occasionally occurs in the acrosome, whereas CifB localizes to the acrosome in all of the mature sperms; (iii) Cifs increase histone retention in developing spermatids and decrease protamine levels in the mature sperms; (iv) During copulation, both Cif proteins transfer with the mature sperm exhibiting reduced protamine levels; (v) In the ovaries, CifA occurs in nuclei of germline stem cells and colocalizes with *Wolbachia* in the nurse cell cytoplasm; (vi) CifA is absent in the embryos, and thus rescue may occur independently of CifA's presence; (vii) Both CI and rescue are dependent upon a bipartite nuclear localization signal (bNLS) in CifA that impacts nuclear localization. Taken together, we demonstrate the first case, to our knowledge, in which prophage WO-encoded Cif proteins invade gametic nuclei to modify chromatin integrity at the histone to protamine transition stage. Results resolve debate on the mechanistic basis of CI by generally supporting the Host Modification model in the *w*Mel-infected *D. melanogaster* system.

Results and Discussion

CifA and CifB invade sperm nuclei during spermatogenesis and spermiogenesis

To evaluate the cellular localization of the Cif proteins, we generated monospecific polyclonal antibodies for visualizing the proteins in reproductive tissues (Fig S1). In *D. melanogaster* males, the sperm morphogenesis process is subdivided into two events (i) Spermatogenesis including mitotic amplification and meiotic phases, and (ii) Spermiogenesis, a post-meiotic phase. During spermatogenesis, the germline stem cell undergoes four rounds of synchronous mitotic divisions to produce 16 precursor cells called spermatogonia. The spermatogonia then grow and become spermatocytes [30]. After the growth phase, the spermatocytes divide by meiosis and differentiate into 64 haploid round onion spermatids. Post-meiosis, the round sperm nuclei elongate to gradually change their shape accompanied by reorganization of the chromatin during the canoe stage [31]. This results in an individualization complex forming slim, needle-shaped sperm nuclei with reduced volume [30,31]. Elongation and individualization of the spermatids is the final stage of spermiogenesis, after which the mature sperms are transported to the seminal vesicle [30,32].

CifA, but not CifB, localizes in the germline stem cells at the apical end of <8 hr old *w*Mel+ and all *cifA* and *cifB* transgene expressing testes (Fig 1, Fig S2). CifA and CifB were both detected in the nuclei of mitotic spermatogonium and spermatocytes. CifA is more abundant than CifB in the spermatogonium stage (Fig S3A, Table S1). In the post-meiotic round onion spermatids, clusters of both CifA and CifB are adjacent to the nuclei. In the elongating canoe-shaped spermatids, CifA and CifB localize to the acrosome, which is the apical position next to the nucleus (Fig 1, Fig S1). CifB is present in all of the spermatid nuclei, whereas CifA is present on an average in 39% of the elongating spermatids per sperm bundle (Fig S3B). During the

93 elongating canoe stage, chromatin-bound histones are typically removed and replaced with
94 protamines to yield compact nuclear packaging and chromatin reorganization of sperms [31].
95 After nuclear compaction is complete, neither of the Cif proteins are detectable in late spermatid
96 needle-shaped nuclei (Fig 1) and in the mature sperms from the seminal vesicle (Fig S4),
97 indicating either the Cif proteins are fully stripped, or they might not be accessible by the
98 antibodies when the chromatin is tightly compacted [33,34]. To evaluate Cif presence/absence in
99 the mature sperm, we decondensed sperms after isolations from seminal vesicles of <8 hr old
100 males (see methods) and stained them with the respective Cif antibodies. CifA is common along
101 sperm tails in a speckled pattern (Fig 1, Fig S1) and infrequently present in the acrosome region,
102 on average in 45% or 0% of the mature sperm heads depending upon the sampled seminal
103 vesicles (Fig S3B). CifB is present in all of the acrosomal tips of the sperms and not localized to
104 the sperm tails (Fig 1, Fig S1).

105 During spermatogenesis, *Wolbachia* are stripped into the cytoplasmic waste bags, which
106 eliminate excess cytoplasmic material during the process of spermatid elongation [23]. Here, we
107 show that some CifA and CifB proteins are also stripped by the individualization complex into
108 the cytoplasmic waste bag (Fig S5). Since *Wolbachia* are not present in the mature sperms
109 [35,36], these data suggest that the Cif proteins exit *Wolbachia* cells during spermatogenesis to
110 interact with and modify sperm DNA (see below). Taken together, these findings demonstrate
111 CifA and CifB proteins access and interact with the nuclei of developing *Drosophila* sperm.

112

113 *Cifs cause abnormal histone retention and protamine deficiency during spermatogenesis*

114 Since the Cifs localize to sperm nuclei during spermatogenesis, we hypothesized that
115 they may interact with sperm nuclear DNA to impact genome integrity of developing sperm in

testes – a central prediction of the Host Modification model of CI [11,29]. At the histone-to-protamine transition stage during spermatogenesis [37], histones normally undergo various post-translational modifications (PTMs) for removal and replacement by smaller protamines for tight chromatin reorganization [37–40]. Lack of PTMs can lead to histone-bound chromatin with improper protamine deposition that causes paternal chromatin defects, male infertility, and embryonic lethality [27,41,42].

Utilizing a core histone antibody, we investigated histone abundance within spermatid bundles at the late canoe stage in CI- and non-CI causing males. We show significantly increased histone retention in both *w*Mel+ and *cifAB*-expressing testes from <8 hr old males compared to the negative controls (Fig 2A, Fig S6, Table S1). Single transgenic expression showed significantly less histone retaining bundles at this stage (Fig S7A, Table S1). To detect if abnormal histone retention is linked with protamine deficiency in mature sperms, we next used the fluorochrome chromomycin A3 (CMA3) stain that fluoresces upon binding to protamine-deficient regions of sperm DNA [43,44]. We show that mature sperms isolated from wild-type seminal vesicles of young (high CI-inducing) *w*Mel+ males exhibit increased protamine deficiency relative to *w*Mel- males (Fig 2B, Table S1). As a positive control, sperm isolated from <8 hr old males with a Protamine A and B knockout mutant, both in the presence (ΔProt+) and absence (ΔProt-) of *Wolbachia,* also exhibit a significant increase in fluorescence relative to *w*Mel- (Fig S8A, Table S1). Moreover, a key outcome of higher protamine deficiency in ΔProt+ males with *Wolbachia* is an increase in *w*Mel+ CI compared to wild type *w*Mel+ CI (Fig S8B, Table S2). These findings indicate an additive effect of the protamine deficiency by *Wolbachia* and ΔProt knock outs on CI penetrance. Notably, ΔProt- males do not recapitulate CI on their own; thus, the protamine deficiency is not the sole cause of CI but works in conjunction with

other modifications by *Wolbachia*. Consistent with these results, 7-day old *w*Mel+ males that express almost no CI (Fig S8C, Fig S8D, Table S2) exhibit a similarly weak protamine deficiency level to *w*Mel- males, as expected. Moreover, transgene analyses specify both single and dual expression of CifA and CifB cause protamine deficiencies at significantly higher levels than negative controls of *w*Mel- and a non-CI transgene (Fig S7B, Table S1). Since singly expressed Cifs do not cause CI in *D. melanogaster* [16] (Fig S7C, Table S2), thus the additive effects on the protamine deficiency and/or histone retention due to abnormal PTMs may be required to fully establish CI. Interestingly, post-fertilization delays in maternal H3.3 histone deposition occur in CI embryos [45]; thus, we propose that a genome integrity network involving histones, protamines, and possibly other factors in the gametes may be a common and defining feature underpinning the onset of CI and rescue.

Cifs cause a paternally-transferred protamine deficiency

To investigate if Cif proteins or the genome integrity modifications are paternally-transferred to the female reproductive tract, we performed single male:female pairwise mating of CI and rescue crosses and then dissected female tissues for marker visualizations. After 4 hrs of mating, we isolated the whole uterus (Fig 3A) including the sperm storage organs - spermathecae (SP) and seminal receptacle (SR) - of mated females and performed sperm decondensation, antibody staining, and microscopy. We report two key results. First, both CifA and CifB proteins travel with the sperms transferred to *Wolbachia*-free females (Fig 3B). Second, the sperm protamine deficiency induced by *w*Mel+ and *cifAB*-expressing males transfers and persists in the sperms isolated from SP and SR of *Wolbachia*-free females (Fig 3C, Fig 3D, Table S1), thus indicating transmission of the paternal chromatin-packaging defect to females together with the

Cifs. In summary, the findings connect the first CI-associated, paternally-transferred sperm modification with the activity of *Wolbachia* and the Cifs themselves, and they support the Host Modification model since a lasting Cif-induced sperm modification is established in the testes and transferred with the Cif proteins to the female reproductive tract.

CifA localizes to ovarian germline nuclei and colocalizes with Wolbachia in the cytoplasm

Expression of *cifA* alone in the ovaries rescues CI [16,17]. Using CifA antibodies, we show that in both *w*Mel+ and *cifA* expressing ovaries, CifA protein localizes to the cyst DNA in region 1 of the germarium (Fig 4A), indicative of nuclear access in ovaries similar to that in testes (Fig 1). Cystoblast in the germarium undergoes rounds of mitotic divisions to produce oocyte and nurse cells [46,47]. Along egg chamber stages 2-8 of *w*Mel+ females, CifA colocalizes with *Wolbachia* in the nurse cells and oocyte cytoplasm (Fig 4A). While *Wolbachia* was still detected in the stage 10 egg chamber, CifA was not present. In *cifA* expressing females, CifA was primarily detected in the germarium and cytoplasm of the early egg chambers (Fig 4A). Presence of high levels of CifA in the egg is proposed to rescue CI. Thus, we hypothesized that loading of CifA protein and/or maternally-derived proteins/transcripts into the oocyte may enable CifA's interaction with the embryonic pronuclei and thus rescue. Notably, we did not detect CifA in ~30-60 min old embryos obtained from the rescue cross (Fig 4B), though positive control histone signals were detected colocalizing with host DNA, suggesting that CifA ovarian expression may impart rescue-capable egg modifications that eventually rescue the fertilized embryo from CI sperms. Taken together, CifA localization in ovaries suggests that future research may focus on how interactions with nuclear DNA enable rescue by either altering chromatin remodeling or impacting maternally-derived products that are essential for repairing

paternal chromatin defects and consequently embryogenesis. This finding is also consistent with a Host Modification model for rescue.

Both CI and rescue are dependent upon a CifA bipartite nuclear localization signal

Based on cNLS mapping tool for nuclear localization signals [48], CifA amino acids notably harbor a predicted bipartite nuclear localization sequence (bNLS) (Table S3) in the most conserved region of the protein [13,49,50] that is under strong purifying selection [17]. As bNLSs bind to the extended surface groove of nuclear transport protein importin-α, also known as karyopherin-α [51], we hypothesized that sperm nuclear localization of CifA and CI and rescue are dependent on the bNLS. To test this hypothesis, we mutagenized two bNLS sequences with alanine substitutions (aa189-190 for NLS1 (denoted $cifA_{189}$), aa224-225 for NLS2 (denoted $cifA_{224}$)), and we additionally deleted the entire bNLS region ($cifA_{\Delta bNLS}$) (Fig 5A). The bNLS deletion also corresponds to the weakly predicted catalase-rel domain in CifA [49,50].

Each bNLS mutant, individually and together ($cifA_{189;224}$), was dually expressed in testes with transgenic *cifB* to assess CI and singly expressed in females to assess rescue. Transgenic $cifA_{189}$ expression yielded a significant reduction in CI (~20%) and rescue (~35%) as we previously reported (Fig 5B, Fig 5C) [50]. Conversely, transgenic $cifA_{224}$ expression showed no significant difference from the controls in either CI or rescue, suggesting this region has little to no impact and the 189 site alone is crucial for CI and rescue phenomenon. However, when both mutants are expressed in $cifA_{189;224}$ or when the entire bNLS is deleted, CI and rescue are strongly inhibited (Fig 5B, Fig 5C). These results highlight the importance of the bNLS in inducing CI as well as rescue. To determine if the lack of CI induction is due to non-nuclear localization of CifA protein, we used the deletion mutant $cifA_{\Delta bNLS}$ with wild type *cifB* to

demonstrate that it mislocalizes to the cytoplasm of onion stage spermatids rather than the nuclei (Fig 5D). Additionally, to test if lack of bNLS can impact sperm genomic integrity, we performed CMA3 based protamine-deficiency assay (as described above) and found reduced protamine deficiency levels due to non CI-causing *cifA*$_{\Delta bNLS}$*;B* line compared to CI-causing *cifAB* (Fig S9, Table S1). Overall, these data provide previously unknown findings that a functional bNLS and thus CifA nuclear localization are required for CI and rescue.

Conclusions

Discovery of nuclear-targeting Cif proteins in fly gametes establishes new insights on the incipient cell biological and genomic steps that underpin a worldwide symbiotic drive system with relevance to arthropod speciation and pest control [11]. As there are no previous reports of phage proteins invading animal gametic nuclei and impairing the histone-to-protamine transition during spermatogenesis, the findings have significant implications for expanding understanding of the tripartite cell biology of prophage-bacteria-eukaryote interactions to include the realm of animal reproduction. In addition to disentangling the germline events of the Cif proteins that control gametogenesis and embryogenesis, the evidence specifies that the Cif proteins modify sperm genomic integrity and paternally transfer, but they themselves do not bind each other in the embryo. These findings strongly support the Host Modification model of CI.

Material and Methods

Cif proteins antibody development

Conserved amino acid regions of CifA and CifB proteins from *w*Mel *Wolbachia* were previously identified [49]. Using these regions, monospecific polyclonal antibodies were commercially generated by Pacific Immunology through injection of three synthesized and conserved short (20 aa) peptides for each protein into rabbits. Sequences of peptides were Cys-EYFYNQLEEKDKEKKLTE for CifA, and Cys-DENPPENLLSDQTRENFRR for CifB. The resulting α-CifA and α-CifB antibodies were evaluated using an enzyme-linked immunosorbent assay, and titers were determined to be higher than 1:500,000 for each antibody. Using standard protocols of the Invitrogen WesternDot kit, antibody specificity to *w*Mel+ samples was verified using western blots (1:1000-fold antibody dilution) on protein isolated from homogenates of 50 testes pairs (0-8 hour old males) and 10 ovary pairs (6 day old females) from *w*Mel+ (positive), *w*Mel- (negative control), and *cifAB* transgenic (positive) flies. The correct size band was only detected from *w*Mel+ and *cifAB* reproductive tissues (Fig S1). Because the antibodies were generated in the same animal, all subsequent labeling was done with individual antibodies.

NLS identification

CifA amino acid sequences from known *Wolbachia* and close relatives were input into the cNLS Mapper software [52] to identify putative NLS sequences within each protein (Table S3). cNLS Mapper identifies sequences specific to the importin α/β pathway. A cut-off score of 4 was applied to all sequences. Higher scores indicate stronger NLS activities. Scores >8 indicate exclusive localization to the nucleus, 7-8 indicate partial localization to the nucleus, 3-5 indicate localization to both the nucleus and the cytoplasm, and score 1-2 indicate localization exclusively to the cytoplasm. Predicted NLS sequences are divided into monopartite and

bipartite classes. Monopartite NLSs contain a single region of basic residues, and bipartite NLSs contain two regions of basic residues separated by a linker region.

Development of transgenic lines

A *cifA* variant was synthesized de novo at GenScript and cloned into a pUC57 plasmid as described previously [50]. Site-directed mutagenesis was performed by GenScript to produce the mutants outlined in Figure 5. The *cifA189* variant was first described in Shropshire et al. [50] as *cifA*$_2$. UAS transgenic *cifA* mutant flies were then generated using previously established protocols [13]. Briefly, GenScript sub-cloned each gene into the pTIGER plasmid, a pUASp-based vector designed for germline-specific expression. Transgenes were then integrated into y^1 M{vas-int.Dm}ZH-2A w*; P{CaryP}attP40 attachment sites into the *D. melanogaster* genome using PhiC31 integrase via embryonic injections by BestGene. At least 200 embryos were injected per transgenic construct, and successful transformants were identified based on red eye color gene included on the pTIGER plasmid containing the transgene. All sequences are reported in Table S4.

Hatch rates

Parental flies were either wild type uninfected (*w*Mel-) or infected (*w*Mel+) with *Wolbachia* or transgene-expressing with no *Wolbachia* infection. Uninfected transgenic flies were generated previously [13,17]. Paternal grandmother age was controlled to 9-11 days for expression of naturally high penetrance of *w*Mel CI [53]. Parental transgenic males were generated through crossing *nanos*-Gal4:VP16 virgin females (aged 9-11 days) to UAS-*cif* transgenic, uninfected males [53]. Mothers were aged 6-9 days before crossing, while father

276 males first emerged between 0-8 hours were used in hatch rates and tissue collections to control
277 for the younger brother effect associated with lower CI penetrance [13].

278 Hatch rates were set up as described previously [13,17]. Briefly, a male and female pair
279 was placed in an 8oz, round bottom, polypropylene *Drosophila* stock bottle with a grape juice-
280 agar plate containing a small amount of yeast placed at the base and secured with tape. These
281 bottles were then placed in a 25°C incubator overnight to allow for courting and mating. The
282 following day, these plates were discarded and replaced with new grape juice-agar plates with
283 fresh yeast. After an additional 24 hours, the plates were removed, and the embryos were
284 counted. The embryo plates were then incubated for 36 hours at 25°C before the total number of
285 unhatched embryos were counted. Any crosses with fewer than 25 embryos laid were discarded
286 from the analyses. Statistical significance ($p<0.05$) was determined by a Kruskal-Wallis test and
287 Dunn's multiple test correction in GraphPad Prism 7. All p-values are listed in Table S2.

288

289 *Immunofluorescence: testes and seminal vesicles*

290 Siblings from the hatch rate (males 0-8 hours) were collected for testes dissection.
291 Tissues were fixed in 4% formaldehyde in PBS-T for 30 min at room temperature and washed in
292 1x PBS-T three times for 5 min each. Tissues were then blocked in 1% BSA in PBS-T for 1 hour
293 at room temperature. They were then incubated with 1° antibody (α-CifA 1:500 OR α-CifB
294 1:500) overnight at 4°C rotating. After washing in 1X PBS-T three times for 5 min each at room
295 temperature, they were incubated with 2° antibody (AlexaFluor 592) for 4 hours at room
296 temperature in the dark. Tissues were then washed three times for 5 minutes each in 1X PBS-T
297 and mounted on slides. To stain the nuclear DNA, 0.2mg/mL of DAPI was added to the
298 mounting media before the coverslip was gently placed over the tissue and excess liquid wiped

299 away. Slides were allowed to dry overnight in the dark before viewing on the Zeiss LSM 880
300 confocal microscope. All images were acquired with the same parameters for each line and
301 processed in ImageJ as described in [54].
302
303 *Decondensation of Mature Sperm Nuclei*
304 Squashed seminal vesicles collected from male flies (aged 0-8 hours) were treated with
305 10 mM DTT, 0.2% Triton X-100, and 400 U heparin in 1X PBS for 30 min [33]. The slides were
306 then washed quickly in 1X PBS before immunofluorescence staining (see above).
307
308 *Immunofluorescence: Histones*
309 Testes from male flies (aged 0-8 hours) were fixed and stained as described above for
310 testes. The tissues were stained with a core histone antibody (MABE71) (1:1000) and imaged on
311 a Keyence BZ-800 microscope. Total late canoe stage sperm bundles were quantified in each
312 testis, and those that retained histones were determined. Ratios of late canoe stage bundles
313 containing histones relative to total bundles from each individual testis were graphed in
314 GraphPad Prism 7. Statistical significance ($p<0.05$) were determined by pairwise comparisons
315 based on Kolmogorov-Smirnov test and multiple comparisons based on a Kruskal-Wallis test
316 and Dunn's multiple test correction in GraphPad Prism 7.
317
318 *Sperm isolation and Chromomycin A3 staining*
319 Seminal vesicles were collected from male flies (aged 0-8 hours for 1-day old flies and 7-
320 days for older flies) and placed on a microscope slide in 1X PBS. Sperm was extracted on the
321 slide using forceps and fixed in 3:1 vol/vol methanol:acetic acid at 4°C for 20 min. Excess

322 solution was then removed, and the slide was air dried. Each slide was treated in the dark for 20
323 min with 0.25mg/mL of CMA3 in McIlvain's buffer, pH 7.0, with 10mM MgCl2. Sperm was
324 then washed in 1x PBS, mounted, and imaged using a Keyence BZ-X700 Fluorescence
325 microscope. All images were acquired with the same parameters for each line and did not
326 undergo significant alteration. Fluorescence quantification was performed by scoring fluorescent
327 pixels in arbitrary units (A.U.) within individual sperm heads using ImageJ as per the details
328 described in [54], and calculated fluorescence intensity per sperm head was graphed. Statistical
329 significance ($p<0.05$) was determined by a Kruskal-Wallis test and Dunn's multiple test
330 correction in GraphPad Prism 7. All of the experiments involving CMA3 staining were
331 performed at 21^0C instead of 25^0C. CI hatch rate assays were run in parallel to ensure that CI and
332 rescue phenotypes are not impacted due to changed temperature conditions.
333
334 *Immunofluorescence: ovaries*
335 Ovaries from females (6 days old) were dissected in PBS on ice and processed as
336 described previously [55]. Tissues were then blocked in 1% BSA in PBS-T for 1 hour at room
337 temperature. They were then incubated with 1° antibody (α-CifA 1:500 OR α-CifB 1:500)
338 overnight at 4°C rotating. For staining *Wolbachia*, a polyclonal antibody against ftsZ protein
339 generated in rabbit was used at 1:150 dilution (a kind gift from Dr. Irene Newton). After washing
340 in 1X PBS-T three times for 5 min each at room temperature, they were incubated with 2°
341 antibody (AlexaFluor 592) for 4 hours at room temperature in the dark. Tissues were then
342 washed three times for 5 minutes each in 1X PBS and mounted on slides. To stain the nuclear
343 DNA, 0.2mg/mL of DAPI was added to the mounting media before the coverslip was gently

placed over the tissue and excess liquid wiped away. Slides were allowed to dry overnight in the dark before viewing on the Zeiss LSM 880 confocal microscope.

Immunofluorescence: embryos

After 24 hours of mating, plates were switched, and embryos were collected every 30 minutes. Embryos were collected in a 100μm mesh basket in embryo wash solution. To remove the chorion, the basket was placed in 50% bleach for 3 min and then rinsed with 1X PBS. The embryos were then transferred to 50:50 4% paraformaldehyde (PFA) and heptane in a microcentrifuge tube and rotated for 20 min at room temperature. Tubes were then removed from the rotator, and the heptane and PFA were allowed to separate before the bottom PFA phase was carefully removed. Methanol was added to the remaining heptane, and the tube was shaken vigorously for 20 seconds before the embryos settled to the bottom and solution was removed. A new volume of methanol was added to the embryos, and they were allowed to settle to the bottom of the tube. Methanol was removed, and all blocking, staining, and imaging steps were carried out for testes and ovary tissues above.

Acknowledgments: The authors thank Jennifer Battle for her assistance in fly collections and staining for sperm integrity assays, Alex Mansueto for his assistance in hatch rates, and both Sarah Bordenstein and Dylan Shropshire for providing helpful feedback on the manuscript. We thank Dr. Irene Newton for providing *Wolbachia* antibody and Dr. Janna McLean for sending the Protamine mutant fly line for conducting the experiments.

Funding: Digestive Disease Research Center Scholarships S1848284, S1848300, S1883559, Vanderbilt-Ingram Cancer Center Scholarships S1871288, S1848887, S1848952, National Institutes of Health Awards R01 AI132581 and AI143725 to S.R.B., F32 Ruth Kirschstein Postdoctoral Fellowship to B.A.L., and the Vanderbilt Microbiome Initiative to S.R.B.

Author contributions: Conceptualization, B.A.L. and S.R.B.; Methodology, B.A.L., R.K. and S.R.B.; Investigation, B.A.L., R.K., and I.T.R.; Writing – Original Draft, B.A.L., R.K. and S.R.B.; Writing – Review & Editing, B.A.L., R.K., I.T.R. and S.R.B.; Funding Acquisition, B.A.L. and S.R.B.; Resources, S.R.B.; Supervision, S.R.B.

Competing interests: Authors declare no competing interests.

Data and materials availability: All data are available in the main text or the supplementary materials. Unique biological materials will be available upon request.

References:

1. Bordenstein SR, Ohara FP, Werren JH. Wolbachia-induced incompatibility precedes other hybrid incompatibilities in Nasonia. Nature. 2001;409: 707–710. doi:10.1038/35055543

2. Charlat S, Hurst GDD, Merçot H. Evolutionary consequences of Wolbachia infections. Trends Genet. 2003;19: 217–223. doi:10.1016/S0168-9525(03)00024-6

3. Jaenike J, Dyer KA, Cornish C, Minhas MS. Asymmetrical reinforcement and Wolbachia infection in Drosophila. PLoS Biol. 2006;4: 1852–1862. doi:10.1371/journal.pbio.0040325

4. Bian G, Xu Y, Lu P, Xie Y, Xi Z. The Endosymbiotic Bacterium Wolbachia Induces Resistance to Dengue Virus in Aedes aegypti. PLoS Pathog. 2010;6: e1000833. doi:10.1371/journal.ppat.1000833

5. Frentiu FD, Zakir T, Walker T, Popovici J, Pyke AT, van den Hurk A, et al. Limited Dengue Virus Replication in Field-Collected Aedes aegypti Mosquitoes Infected with Wolbachia. PLoS Negl Trop Dis. 2014;8. doi:10.1371/journal.pntd.0002688

6. Walker T, Johnson PH, Moreira LA, Iturbe-Ormaetxe I, Frentiu FD, McMeniman CJ, et al. The wMel Wolbachia strain blocks dengue and invades caged Aedes aegypti populations. Nature. 2011;476: 450–455. doi:10.1038/nature10355

7. Bourtzis K, Dobson SL, Xi Z, Rasgon JL, Calvitti M, Moreira LA, et al. Harnessing mosquito-Wolbachia symbiosis for vector and disease control. Acta Trop. 2014;132. doi:10.1016/j.actatropica.2013.11.004

8. Hughes GL, Koga R, Xue P, Fukatsu T, Rasgon JL. Wolbachia infections are virulent and inhibit the human malaria parasite Plasmodium falciparum in Anopheles gambiae. PLoS Pathog. 2011;7: e1002043. doi:10.1371/journal.ppat.1002043

9. O'Connor L, Plichart C, Sang AC, Brelsfoard CL, Bossin HC, Dobson SL. Open release of male mosquitoes infected with a wolbachia biopesticide: field performance and infection containment. PLoS Negl Trop Dis. 2012;6: e1797. doi:10.1371/journal.pntd.0001797

10. Taylor MJ, Bordenstein SR, Slatko B. Microbe profile: Wolbachia: A sex selector, a viral protector and a target to treat filarial nematodes. Microbiol (United Kingdom). 2018. doi:10.1099/mic.0.000724

11. Shropshire JD, Leigh B, Bordenstein SR, Initiative M. Symbiont-mediated cytoplasmic incompatibility□: What have we learned in 50 years? Elife. 2020; 1–51. doi:10.20944/preprints202008.0350.v1

12. Turelli M. Evolution of incompatibility-inducing microbes and their hosts. Evolution (N Y). 1994;48: 1500–1513. doi:10.1111/j.1558-5646.1994.tb02192.x

13. LePage DP, Metcalf JA, Bordenstein SR, On J, Perlmutter JI, Shropshire JD, et al. Prophage WO genes recapitulate and enhance Wolbachia-induced cytoplasmic incompatibility. Nature. 2017;543: 243–247. doi:10.1038/nature21391

14. Bordenstein SR, Bordenstein SR. Eukaryotic association module in phage WO genomes from Wolbachia. Nat Commun. 2016;7. doi:10.1038/ncomms13155

15. Beckmann JF, Ronau JA, Hochstrasser M. A Wolbachia deubiquitylating enzyme induces cytoplasmic incompatibility. Nat Microbiol. 2017;2. doi:10.1038/nmicrobiol.2017.7

16. Shropshire JD, Bordenstein SR. Two-by-one model of cytoplasmic incompatibility: Synthetic recapitulation by transgenic expression of cifa and cifb in drosophila. PLoS Genet. 2019;15. doi:10.1371/journal.pgen.1008221

17. Shropshire JD, On J, Layton EM, Zhou H, Bordenstein SR. One prophage WO gene

rescues cytoplasmic incompatibility in Drosophila melanogaster. Proc Natl Acad Sci U S A. 2018;115: 4987–4991. doi:10.1073/pnas.1800650115

18. Adams KL, Abernathy DG, Willett BC, Selland EK. Wolbachia cifB induces cytoplasmic incompatibility in the malaria mosquito. 2021. doi:10.1101/2021.04.20.440637

19. Sun G, Zhang M, Chen H, Hochstrasser M. The Wolbachia CinB Nuclease is Sufficient for Induction of Cytoplasmic Incompatibility. bioRxiv. 2021; 2021.10.22.465375. Available: https://www.biorxiv.org/content/10.1101/2021.10.22.465375v1%0Ahttps://www.biorxiv.org/content/10.1101/2021.10.22.465375v1.abstract

20. Yang P, Wu W, Macfarlan TS. Maternal histone variants and their chaperones promote paternal genome activation and boost somatic cell reprogramming. BioEssays. 2015;37: 52–59. doi:10.1002/bies.201400072

21. Landmann F, Orsi GA, Loppin B, Sullivan W. Wolbachia-mediated cytoplasmic incompatibility is associated with impaired histone deposition in the male pronucleus. PLoS Pathog. 2009;5. doi:10.1371/journal.ppat.1000343

22. Lassy CW, Karr TL. Cytological analysis of fertilization and early embryonic development in incompatible crosses of Drosophila simulans. Mech Dev. 1996;57: 47–58. doi:10.1016/0925-4773(96)00527-8

23. Serbus LR, Casper-Lindley C, Landmann F, Sullivan W. The genetics and cell biology of Wolbachia-host interactions. Annu Rev Genet. 2008;42: 683–707. doi:10.1146/annurev.genet.41.110306.130354

24. Tram U, Sullivan W. Role of delayed nuclear envelope breakdown and mitosis in Wolbachia-induced cytoplasmic incompatibility. Science (80-). 2002;296: 1124–1126.

448 doi:10.1126/science.1070536

449 25. Tram U, Fredrick K, Werren JH, Sullivan W. Paternal chromosome segregation during the
450 first mitotic division determines Wolbachia-induced cytoplasmic incompatibility
451 phenotype. J Cell Sci. 2006;119: 3655–3663. doi:10.1242/jcs.03095

452 26. Callaini G, Riparbelli MG, Giordano R, Dallai R. Mitotic defects associated with
453 cytoplasmic incompatibility in Drosophila simulans. J Invertebr Pathol. 1996;67: 55–64.
454 doi:10.1006/jipa.1996.0009

455 27. Callaini G, Dallai R, Riparbelli MG. Wolbachia-induced delay of paternal chromatin
456 condensation does not prevent maternal chromosomes from entering anaphase in
457 incompatible crosses of Drosophila simulans. J Cell Sci. 1997;110 (Pt 2: 271–280.

458 28. Beckmann JF, Bonneau M, Chen H, Hochstrasser M, Poinsot D, Merçot H, et al. The
459 Toxin–Antidote Model of Cytoplasmic Incompatibility: Genetics and Evolutionary
460 Implications. Trends in Genetics. 2019. pp. 175–185. doi:10.1016/j.tig.2018.12.004

461 29. Shropshire JD, Leigh B, Bordenstein SR, Duplouy A, Riegler M, Brownlie JC, et al.
462 Models and Nomenclature for Cytoplasmic Incompatibility: Caution over Premature
463 Conclusions – A Response to Beckmann et al. Trends in Genetics. 2019. pp. 397–399.
464 doi:10.1016/j.tig.2019.03.004

465 30. Fuller M. The Development of Drosophila melanogaster. Cold Spring Harbor Laboratory
466 Press. Spermatogenesis. 1993; 71–147.

467 31. Jayaramaiah Raja S, Renkawitz-Pohl R. Replacement by Drosophila melanogaster
468 Protamines and Mst77F of Histones during Chromatin Condensation in Late Spermatids
469 and Role of Sesame in the Removal of These Proteins from the Male Pronucleus . Mol
470 Cell Biol. 2005;25: 6165–6177. doi:10.1128/mcb.25.14.6165-6177.2005

32. Fabian L, Brill JA. Drosophila spermiogenesis. Spermatogenesis. 2012;2: 197–212. doi:10.4161/spmg.21798

33. Eren-Ghiani Z, Rathke C, Theofel I, Renkawitz-Pohl R. Prtl99C Acts Together with Protamines and Safeguards Male Fertility in Drosophila. Cell Rep. 2015;13: 2327–2335. doi:10.1016/j.celrep.2015.11.023

34. Bonnefoy E, Orsi GA, Couble P, Loppin B. The essential role of Drosophila HIRA for de novo assembly of paternal chromatin at fertilization. PLoS Genet. 2007;3: 1991–2006. doi:10.1371/journal.pgen.0030182

35. Bressac C, Rousset F. The reproductive incompatibility system in Drosophila simulans: Dapi-staining analysis of the Wolbachia symbionts in sperm cysts. J Invertebr Pathol. 1993;61: 226–230. doi:10.1006/jipa.1993.1044

36. Clark ME, Veneti Z, Bourtzis K, Karr TL. The distribution and proliferation of the intracellular bacteria Wolbachia during spermatogenesis in Drosophila. Mech Dev. 2002;111: 3–15. Available: http://www.ncbi.nlm.nih.gov/pubmed/11804774

37. Rathke C, Baarends WM, Jayaramaiah-Raja S, Bartkuhn M, Renkawitz R, Renkawitz-Pohl R. Transition from a nucleosome-based to a protamine-based chromatin configuration during spermiogenesis in Drosophila. J Cell Sci. 2007;120: 1689–1700. doi:10.1242/jcs.004663

38. Brunner AM, Nanni P, Mansuy IM. Epigenetic marking of sperm by post-translational modification of histones and protamines. Epigenetics and Chromatin. 2014;7. doi:10.1186/1756-8935-7-2

39. Luense LJ, Donahue G, Lin-Shiao E, Rangel R, Weller AH, Bartolomei MS, et al. Gcn5-Mediated Histone Acetylation Governs Nucleosome Dynamics in Spermiogenesis. Dev

Cell. 2019;51: 745-758.e6. doi:10.1016/j.devcel.2019.10.024

40. Goudarzi A, Shiota H, Rousseaux S, Khochbin S. Genome-scale acetylation-dependent histone eviction during spermatogenesis. J Mol Biol. 2014;426: 3342–3349. doi:10.1016/j.jmb.2014.02.023

41. Fenic I, Sonnack V, Failing K, Bergmann M, Steger K. In vivo effects of histone-deacetylase inhibitor trichostatin-A on murine spermatogenesis. J Androl. 2004;25: 811–818. doi:10.1002/j.1939-4640.2004.tb02859.x

42. Sonnack V, Failing K, Bergmann M, Steger K. Expression of hyperacetylated histone H4 during normal and impaired human spermatogenesis. Andrologia. 2002;34: 384–390. doi:10.1046/j.1439-0272.2002.00524.x

43. Lolis D, Georgiou I, Syrrou M, Zikopoulos K, Konstantelli M, Messinis I. Chromomycin A3-staining as an indicator of protamine deficiency and fertilization. Int J Androl. 1996;19: 23–27. doi:10.1111/j.1365-2605.1996.tb00429.x

44. Kazerooni T, Asadi N, Jadid L, Kazerooni M, Ghanadi A, Ghaffarpasand F, et al. Evaluation of sperm's chromatin quality with acridine orange test, chromomycin A3 and aniline blue staining in couples with unexplained recurrent abortion. J Assist Reprod Genet. 2009;26: 591–596. doi:10.1007/s10815-009-9361-3

45. Landmann F, Orsi GA, Loppin B, Sullivan W. Wolbachia-mediated cytoplasmic incompatibility is associated with impaired histone deposition in the male pronucleus. PLoS Pathog. 2009;5. doi:10.1371/journal.ppat.1000343

46. Ferree PM, Frydman HM, Li JM, Cao J, Wieschaus E, Sullivan W. Wolbachia utilizes host microtubules and Dynein for anterior localization in the Drosophila oocyte. PLoS Pathog. 2005;1: e14. doi:10.1371/journal.ppat.0010014

47. Marlow FL. Maternal Control of Development in Vertebrates. Colloq Ser Dev Biol. 2010;1: 1–196. doi:10.4199/c00023ed1v01y201012deb005

48. Kosugi S, Hasebe M, Tomita M, Yanagawa H. Systematic identification of cell cycle-dependent yeast nucleocytoplasmic shuttling proteins by prediction of composite motifs. Proc Natl Acad Sci U S A. 2009;106: 10171–10176. doi:10.1073/pnas.0900604106

49. Lindsey ARI, Rice DW, Bordenstein SR, Brooks AW, Bordenstein SR, Newton ILG. Evolutionary Genetics of Cytoplasmic Incompatibility Genes cifA and cifB in Prophage WO of Wolbachia. Genome Biol Evol. 2018;10: 434–451. doi:10.1093/gbe/evy012

50. Shropshire JD, Kalra M, Bordenstein SR. Evolution-guided mutagenesis of the cytoplasmic incompatibility proteins: Identifying CifA's complex functional repertoire and new essential regions in CifB. PLoS Pathog. 2020;16: e1008794. doi:10.1371/journal.ppat.1008794

51. Kosugi S, Hasebe M, Matsumura N, Takashima H, Miyamoto-Sato E, Tomita M, et al. Six classes of nuclear localization signals specific to different binding grooves of importinα. J Biol Chem. 2009;284: 478–485. doi:10.1074/jbc.M807017200

52. Zhang B, Ye W, Ye Y, Zhou H, Saeed AFUH, Chen J, et al. Structural insights into Cas13b-guided CRISPR RNA maturation and recognition. Cell Res. 2018;28: 1198–1201. doi:10.1038/s41422-018-0109-4

53. Layton EM, On J, Perlmutter JI, Bordenstein SR, Shropshire JD. Paternal grandmother age affects the strength of Wolbachia-induced cytoplasmic incompatibility in Drosophila melanogaster. MBio. 2019;10. doi:10.1128/mBio.01879-19

54. Kaur R, Martinez J, Rota-Stabelli O, Jiggins FM, Miller WJ. Age, tissue, genotype and virus infection regulate Wolbachia levels in Drosophila. Mol Ecol. 2020;29: 2063–2079.

doi:10.1111/mec.15462

55. Newton ILG, Savytskyy O, Sheehan KB. Wolbachia Utilize Host Actin for Efficient Maternal Transmission in Drosophila melanogaster. PLoS Pathog. 2015;11. doi:10.1371/journal.ppat.1004798

Figure legends

Fig 1. CifA and CifB invade sperm nuclei during spermatogenesis and spermiogenesis. Schematic representation of *Drosophila melanogaster* male reproductive system created by Biorender is shown on the top. Testes (n=20) from <8 hrs old males expressing dual transgenes *nos;cifAB* were dissected and immunostained to visualize CifA (green) and CifB (red) during sperm morphogenesis. DAPI stain (blue) was used to label nuclei. CifA, but not CifB, localizes in the germline stem cells at the apical end of testes. Both CifA and CifB localize in the nuclei of mitotic spermatogonium, spermatocytes and round onion stage spermatids. In the later stages of spermiogenesis, elongating spermatids harbor CifA and CifB at the acrosomal tip of the heads. CifB is present in all canoe-stage spermatid nuclei, whereas CifA is present on average in 39% of spermatids per bundle. Cifs are not accessible by the antibodies in the tightly compacted spermatids at the needle-stage. After decondensing mature sperms isolated from seminal vesicles (see methods), CifA and CifB are detectable in the acrosome regions at varying percentages. CifA is common among sperm tails in a speckled pattern (white arrow) and either present on average in 45% or 0% of the mature sperm heads depending upon the sampled seminal vesicles. CifA's presence in the acrosome region is shown by solid white arrowheads and absence with empty white arrowheads. CifB is present in acrosomal tips of all of the sperms (solid white arrowheads) and does not occur with sperm tails. CifA and CifB localization patterns are similar in wild type (*w*Mel+) line and signals are absent in *Wolbachia*-uninfected (*w*Mel-) negative control line (Fig S2). Some of the CifA and CifB proteins are also stripped by the individualization complex into the cytoplasmic waste bag (Fig S5). The experiment was repeated in two biological replicates.

Fig 2. Cifs cause histone retention in late canoe spermatids and a protamine deficiency in mature sperms. (A) Testes (n=15) from <8 hrs old males of *w*Mel+, *w*Mel- and transgenic *nos;cifAB* lines were dissected and immunostained to visualize and quantify spermatid bundles with histone retention (purple) during late canoe stage of spermatogenesis. DAPI stain (blue) was used to label spermatid nuclei. Total spermatid bundles with DAPI signals and those with retained Histones were manually counted and graphed. Compared to the negative control *w*Mel-, *w*Mel+ *Wolbachia* and dually-expressed *cifAB* transgenic lines show abnormal histone retention in the late canoe stage. Vertical bars represent mean, and error bars represent standard deviation.

Letters indicate statistically significant ($p<0.05$) differences as determined by pairwise comparisons based on Kolmogorov-Smirnov test. (B) Mature sperms isolated from seminal vesicles (n=15) of <8 hr old males reared at 21°C were stained with fluorescent CMA3 (green) for detection of protamine deficiency in each individual sperm nucleus. Individual sperm head intensity was quantified in ImageJ (see methods) and graphed. *w*Mel+ and transgenic *cifAB* lines show enhanced protamine deficiency levels compared to *w*Mel- control. Vertical bars represent mean and error bars represent standard deviation. Letters indicate statistically significant ($p<0.05$) differences as determined by multiple comparisons based on a Kruskal-Wallis test and Dunn's multiple test correction. All of the P-values are reported in Table S1. The experiments were performed in two independent biological replicates and samples were blind-coded for the first run.

Fig 3. CifA, CifB, and the protamine deficiency are transferred with the mature sperm to the female reproductive tract. (A) Schematic representation of *Drosophila melanogaster* female reproductive system. Mature oocytes leave the ovary (OV) and reach the uterus (UT), where they can be fertilized prior to being laid. Sperms from males are stored in specialized organs - spermathecae (SP) and seminal receptacle (SR) shown in the box, which open into the UT for fertilization to occur. Schematic is created with BioRender (B) Transgenic *cifAB*-expressing and *w*Mel- males were crossed to *w*Mel- females. 4 hrs post-fertilization, sperms isolated from females were decondensed and immunostained for localizing CifA (green) and CifB (red). DAPI stain (blue) was used to label nuclei. CifA is absent in sperm heads (empty arrowheads) and puctae are seen along the sperm tails (arrows). CifB is present in apical acrosomal tip of all of the sperm heads (solid arrowheads), with more distant signal in the more decondensed sperm nuclei. No Cifs are present in the sperms transferred from *w*Mel- negative control males. (C) Individual sperm intensity quantification shows that protamine deficiency of sperms from *w*Mel+ and transgenic *cifAB* males persists after transfer in the females compared to *w*Mel- males. Sperm protamine deficiency from transgenic *cifAB* males also persists in the reproductive tract of *w*Mel+ females. Vertical bars represent mean, and error bars represent standard deviation. Letters indicate statistically significant ($p<0.05$) differences as determined by multiple comparisons based on a Kruskal-Wallis test and Dunn's multiple test correction. All of the P-values are reported in Table S1. The experiments were performed in two independent biological replicates. (D) Representative images of CMA3-stained mature sperms (arrows) transferred from *w*Mel-, *w*Mel+ and transgenic *cifAB* males in *w*Mel- and *w*Mel+ female reproductive systems are shown.

Fig 4. CifA localizes to the ovarian germarium and colocalizes with *Wolbachia* in nurse cell cytoplasm. (A) Schematic representation of *Drosophila melanogaster* ovariole at the top illustrates the stages of oogenesis from left to right. Image was created with BioRender. Immunostaining in *Wolbachia*-infected wild type *w*Mel+ line and *Wolbachia*-uninfected transgenic *nos;cifA* line indicates localization of CifA (green) to the cyst DNA (blue labeled with

DAPI) in region 1 of the germarium. In *w*Mel+ line, CifA colocalizes with *Wolbachia* (red) in the nurse cells and oocyte cytoplasm along 2-8 stages of egg chambers. CifA is absent in stage 10 egg chamber, whereas *Wolbachia* signals persist. In the transgenic *cifA* line, we note the observed autofluorescence in green channel outlining the tissue morphology that does not signify CifA signals. (B) Immunofluorescence of CifA (green) in ~30-60 min old embryos in a rescue cross with *Wolbachia*-infected female (*cifAB* male x *w*Mel+ female). Histone antibody labeling core-histones (green) was used as a positive control. Histones signals were detected colocalizing with host DNA, whereas no CifA signals were detected. Embryo periphery is outlined with a dotted white line, and divided nuclei are outlined in white circles.

Fig 5. A nuclear localization signal in CifA is necessary for CI and rescue. (A) Schematic representation of CifA annotation shows the annotated bipartite nuclear localization signal (bNLS) with engineered amino acid substitutions and deletions. (B, C) Hatch rate assays assessed both CI (B) and rescue (C) in flies expressing wild type, transgenic, and mutant *cifA*. Each dot represents the percent of embryos that hatched from a single male and female pair. Sample size is listed in parentheses. Horizontal bars represent median. Letters to the right indicate significant differences determined by a Kruskal-Wallis test and Dunn's multiple comparison test. All the P-values are reported in Table S2. (D) Antibody labeling (green) and DAPI staining of onion stage spermatids in the testes of the bNLS mutant line ($cifA_{\Delta bNLS}$) reveals that the deletion ablates CifA's localization to the nucleus, and CifA thus remains in the surrounding cytoplasm. The experiments were conducted twice.

Supplementary figure legends.

Fig S1. Western blots using Cif antibodies reveal protein bands at the proper size. Western blots were run on protein extracted from both testes and ovaries of wild type infected *w*Mel+, uninfected *w*Mel- and dual *cifAB* expressing transgenic lines. Cifs are absent in *w*Mel- control and present at accurate size in *w*Mel+ and *cifAB* lines.

Fig S2. Cifs invade spermatid nuclei in wild type *w*Mel+ testes and absent in *w*Mel- control line. Testes (n=20) from <8 hrs old males of wild type *w*Mel+ and *w*Mel- lines were dissected and immunostained to visualize CifA (green) and CifB (red) during sperm morphogenesis. DAPI stain (blue) was used to label nuclei. CifA and CifB localization patterns in wild type lines are similar to that of transgenic *cifAB* (Fig 1) and signals are absent in *w*Mel- uninfected control line. The experiment was conducted in parallel to the one shown in Fig 1.

Fig S3. CifA and CifB vary in abundance levels in spermatids and mature sperms. (A) ImageJ-based signal intensity quantification indicates CifA (green) is more abundantly expressed than CifB (red) in the spermatogonium stage of the spermatogenesis. Mean of individual data

points with standard deviation is plotted on the graph. Letters indicate statistically significant ($p<0.05$) differences as determined by pairwise comparisons based on a Mann-Whitney test. P-values are reported in Table S1. (B) In the decondensed mature sperms isolated from seminal vesicles, CifB is present in the acrosomal tip of canoe-shaped spermatids and mature sperm heads, whereas CifA is present in only 40% and 20% of them, respectively. Quantification was performed on the images obtained in Fig 1 data. Each dot represents percentage of Cifs present in spermatids or mature sperms per testes examined.

Fig S4. CifA and CifB are not detectable in the condensed mature sperms in seminal vesicles due to technical limitations. Seminal vesicles (n=20) from <8 hrs old males of transgenic *cifAB*, wild type *w*Mel+ and *w*Mel- lines were dissected and immunostained to visualize CifA (green) and CifB (red) in the mature condensed sperms (indicated by white arrows). DAPI stain (blue) was used to label nuclei. Absence of both CifA and CifB indicates that proteins are not accessible to the antibodies when the sperm chromatin is condensed and tightly packed.

Fig S5. CifA and CifB are also removed in the cytoplasmic waste bag. Testes (n=20) from <8 hrs old males of transgenic *cifAB*, and wild type *w*Mel- lines were dissected and immunostained to visualize CifA (green) and CifB (red) in the cytoplasmic waste bags (WB) that are present near the basal end of sperm tail bundles. Some of the Cif proteins strip down in the WB in *cifAB* line and absent in *w*Mel- control testes. Brightfield is shown to highlight the morphology of sperm tail bundles and waste bags, which are otherwise not visible using Cif antibodies and DAPI stain. The experiment was run in parallel to the ones shown in Fig 1 and Fig S2.

Fig S6. Full uncropped fluorescent images are shown related to Fig 2A.

Fig S7. Individual CifA and CifB expressing lines do not show abnormal histone retention but are protamine deficient. (A) Testes (n=15) from <8 hrs old males of single transgene-expressing lines *cifA*, *cifB* and a non CI-causing control gene *WD0508* were dissected to quantify spermatid bundles with histone retention (purple) during late canoe stage of spermatogenesis. DAPI stain (blue) was used to label spermatid nuclei. Total spermatid bundles with DAPI signals and those with retained Histones were manually counted and graphed. Single transgenic expressing lines showed significantly less histones similar to the negative control *w*Mel- at the late canoe stage. Vertical bars represent mean and error bars represent standard deviation. Letters indicate statistically significant ($p<0.05$) differences as determined by multiple comparisons based on a Kruskal-Wallis test and Dunn's multiple test correction. (B) Mature sperms isolated from seminal vesicles (n=15) of <8 hr old males reared at 21°C were stained with fluorescent CMA3 (green) for detection of protamine deficiency in each individual sperm nucleus. Individual sperm head intensity was quantified in ImageJ (see methods) and graphed. *cifA*- and *cifB*-expressing lines showed significantly higher fluorescence indicative of reduced levels of

protamines compared to *w*Mel- and *WD0508* control lines. Vertical bars represent mean and error bars represent standard deviation. Letters indicate statistically significant ($p<0.05$) differences as determined by multiple comparisons based on a Kruskal-Wallis test and Dunn's multiple test correction. All of the P-values are reported in Table S1. The experiments were performed in parallel to the ones shown in Fig 2. (C) CI hatch rate analyses of transgenic male siblings used in CMA3 assays (Figure 2B, S6) validate that CI crosses (black circles) yielded significant less embryonic hatching compared to non CI-inducing ones, when reared at 21^0C. Letters to the right indicate statistically significant ($p<0.05$) differences as determined by multiple comparisons based on a Kruskal-Wallis test and Dunn's multiple test correction. All of the P-values are reported in Table S2.

Fig S8. Protamine mutants show significantly increased levels of protamine deficiency in mature sperms compared to *w*Mel- flies. (A and C) Sperms from the *Wolbachia*-infected (ΔProt+) and -uninfected (ΔProt-) protamine mutant (w[1118]; ΔMst35B[floxed], Sco/CyO) males exhibit significantly increased CMA3 fluorescence indicative of protamine deficiency compared to both wild type *w*Mel+ and *w*Mel-. 7 day-old *w*Mel+ males that do not cause CI show similar level of protamine levels as of 7 day-old *w*Mel-. Vertical bars represent mean, and error bars represent standard deviation. Letters indicate statistically significant ($p<0.05$) differences as determined by multiple comparisons based on a Kruskal-Wallis test and Dunn's multiple test correction. All of the P-values are reported in Table S1. (B and D) CI hatch rate analyses of male siblings used in CMA3 assays (panel A and C) validate that ΔProt+ males with increased sperm protamine deficiency causes stronger (rescuable) CI levels than *w*Mel+. ΔProt- males do not cause CI. 7d old *w*Mel+ do not induce CI in a manner that correlates with their reduced levels of sperm protamine deficiency. Letters to the right indicate statistically significant ($p<0.05$) differences as determined by pairwise Mann-Whitney test and multiple comparisons calculated using a Kruskal-Wallis test and Dunn's multiple test correction. All of the P-values are reported in Table S2.

Fig S9. Deletion of CifA bNLS reduces protamine deficiency levels. Mature sperms isolated from seminal vesicles (n=15) of <8 hr old males of transgenic *cifA*$_{\Delta bnls}$*B* line shows reduced fluorescence indicative of less Protamine deficiency compared to *cifAB*. To control for any background confounding effects of *nos-Gal4VP16* driver line, *w*Mel- fathers were prior crossed to *nos*- mothers to generate males with *nos;wMel*- genotype. CMA3 fluorescence levels of sperms isolated from *nos;wMel*- males were similar to *w*Mel- wild type lines used in previous assays in this study. Vertical bars represent mean and error bars represent standard deviation. Letters indicate statistically significant ($p<0.05$) differences as determined by multiple comparisons based on a Kruskal-Wallis test and Dunn's multiple test correction. All of the P-values are reported in Table S1.

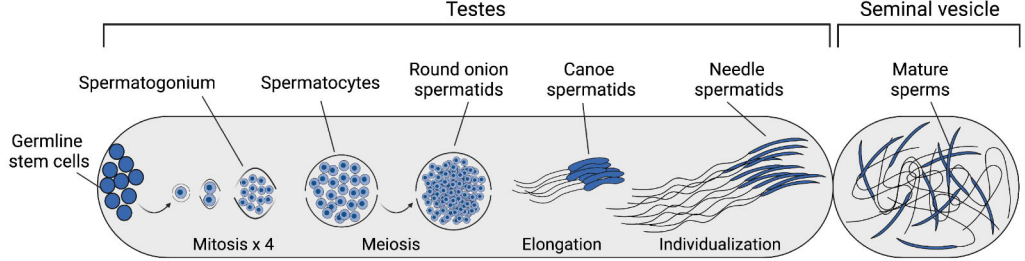
Testes
Seminal vesicle
Spermatogonium
Spermatocytes
Round onion spermatids
Canoe spermatids
Needle spermatids
Mature sperms
Germline stem cells
Mitosis x 4
Meiosis
Elongation
Individualization

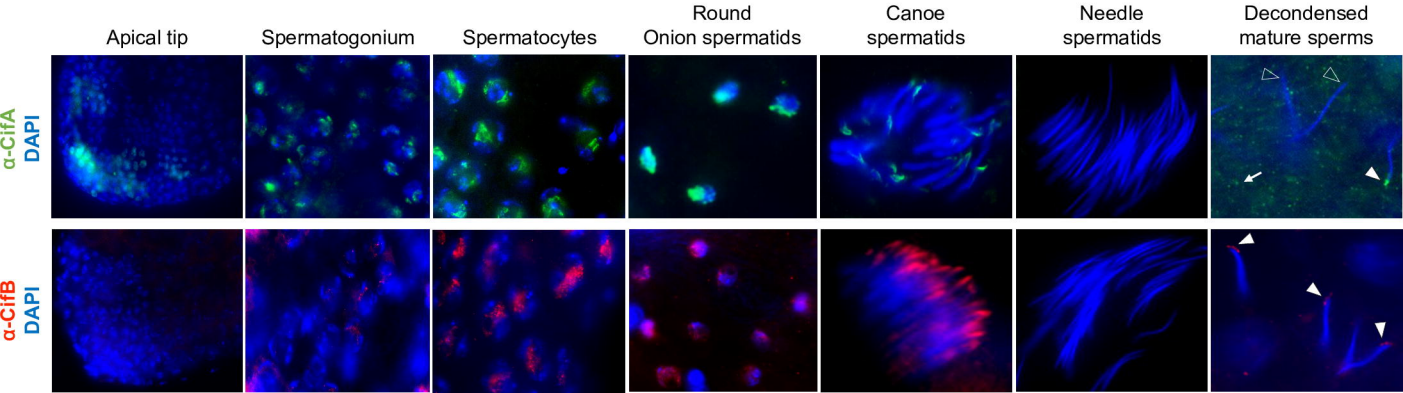
Apical tip
Spermatogonium
Spermatocytes
Round Onion spermatids
Canoe spermatids
Needle spermatids
Decondensed mature sperms
α-CifA
DAPI
α-CifB
DAPI

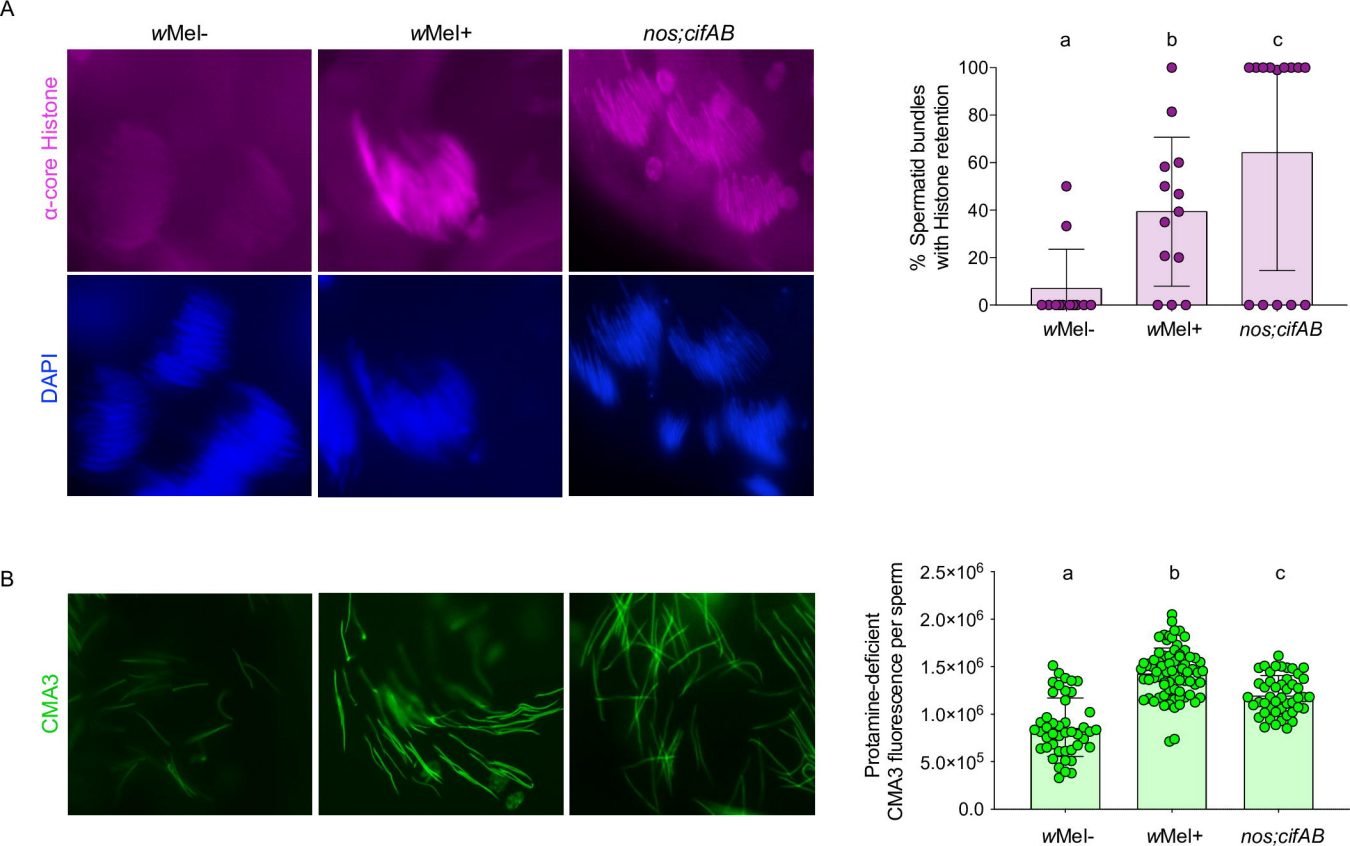
A
wMel-
wMel+
nos;cifAB
α-core Histone
DAPI
% Spermatid bundles with Histone retention
a
b
c
100
80
60
40
20
0
wMel-
wMel+
nos;cifAB
B
CMA3
Protamine-deficient CMA3 fluorescence per sperm
2.5×10^6
2.0×10^6
1.5×10^6
1.0×10^6
5.0×10^5
0.0
a
b
c
wMel-
wMel+
nos;cifAB

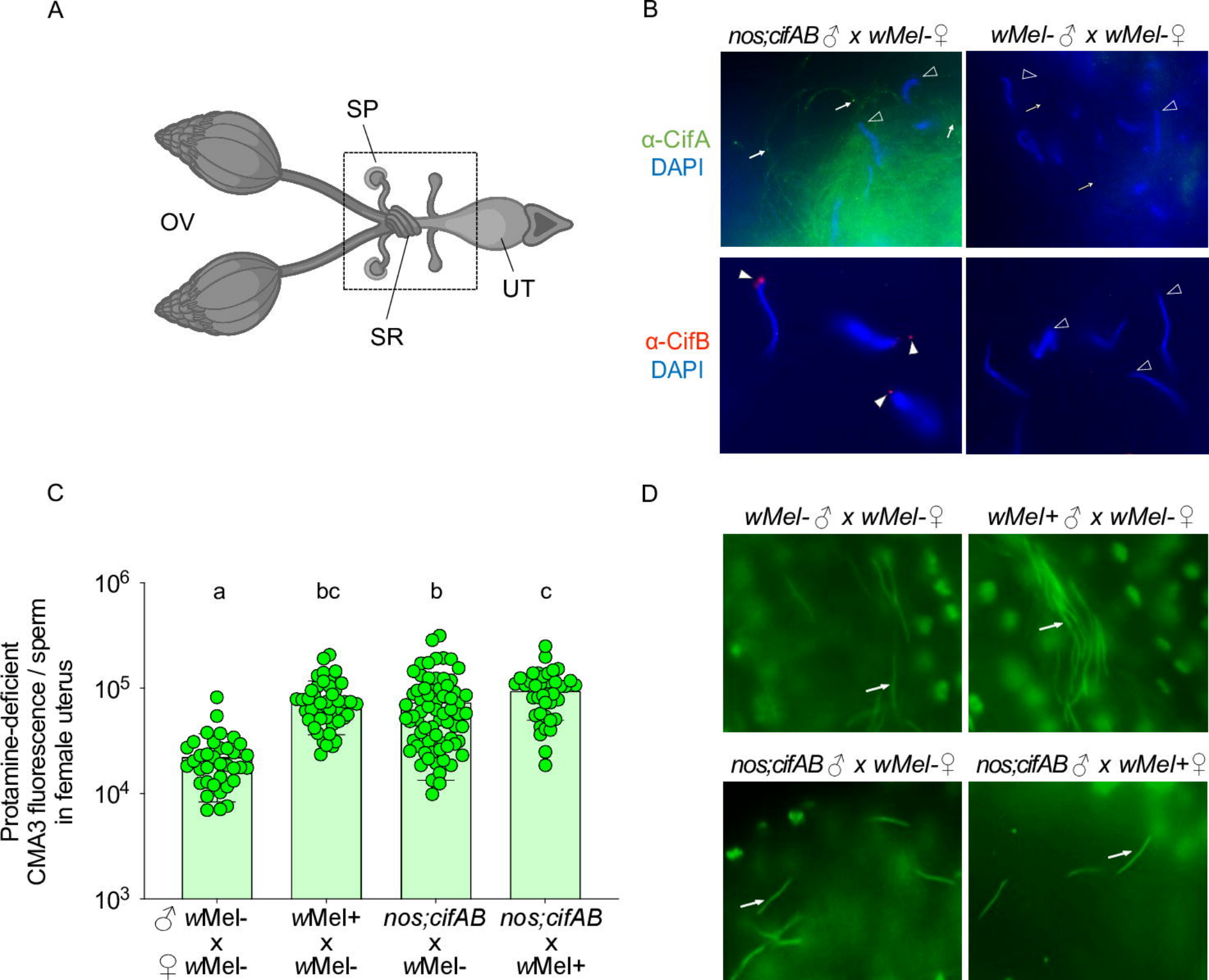
A
SP
OV
UT
SR
B
nos;cifAB ♂ x wMel- ♀
wMel- ♂ x wMel- ♀
α-CifA
DAPI
α-CifB
DAPI
C
Protamine-deficient CMA3 fluorescence / sperm in female uterus
10^6
10^5
10^4
10^3
a
bc
b
c
♂ wMel- x ♀ wMel-
wMel+ x wMel-
nos;cifAB x wMel-
nos;cifAB x wMel+
D
wMel- ♂ x wMel- ♀
wMel+ ♂ x wMel- ♀
nos;cifAB ♂ x wMel- ♀
nos;cifAB ♂ x wMel+ ♀

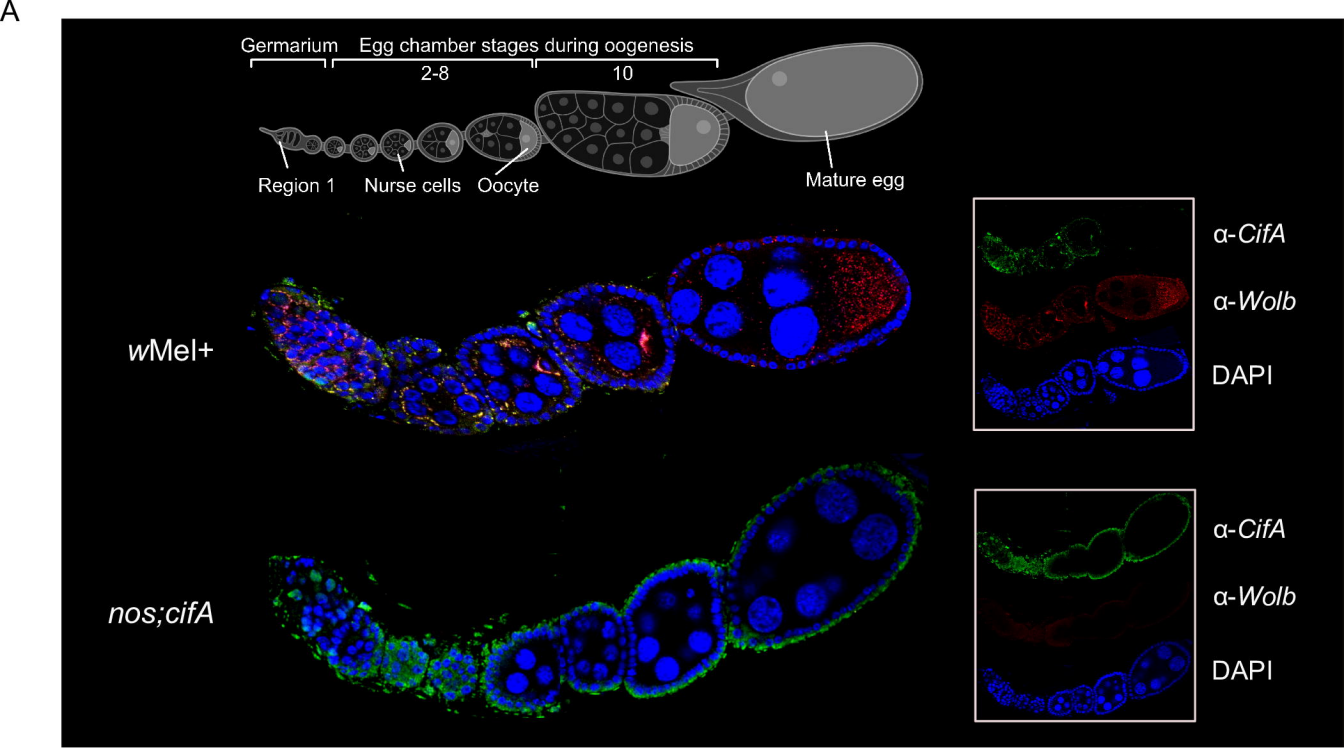
A
Germarium
Egg chamber stages during oogenesis
2-8
10
Region 1
Nurse cells
Oocyte
Mature egg
wMel+
nos;cifA
α-CifA
α-Wolb
DAPI
α-CifA
α-Wolb
DAPI

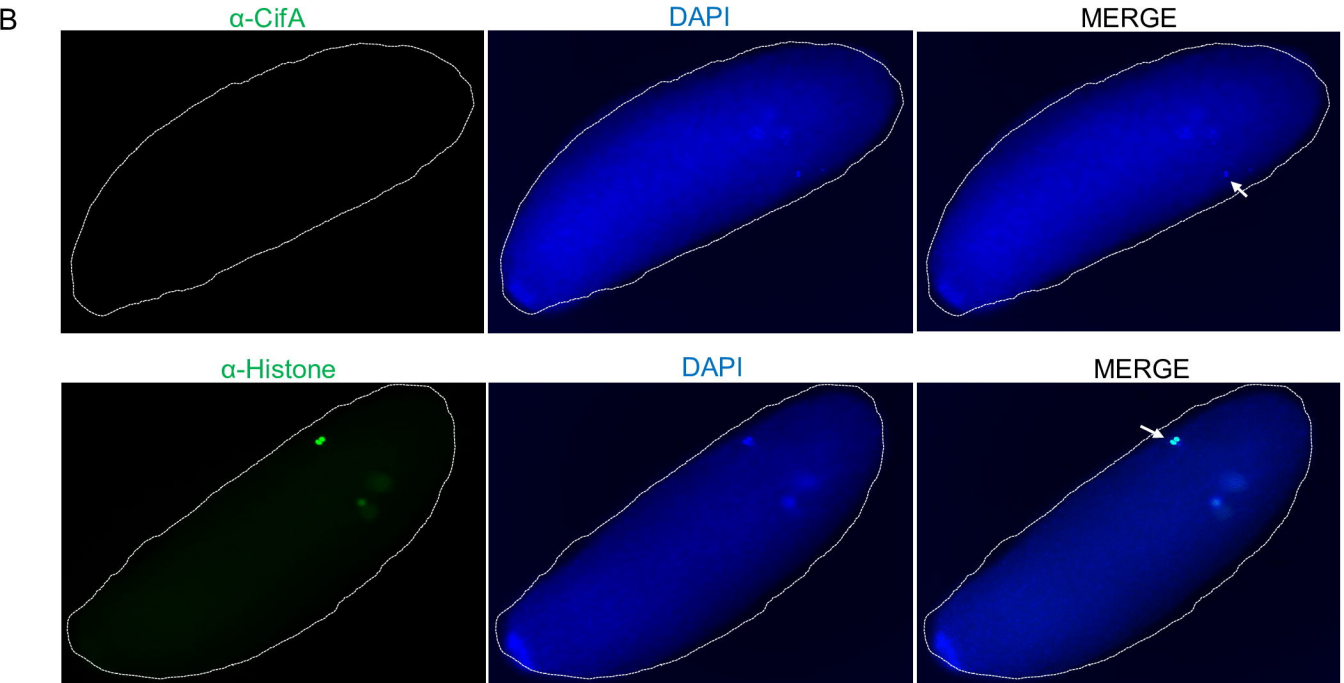
B
α-CifA
DAPI
MERGE
α-Histone
DAPI
MERGE

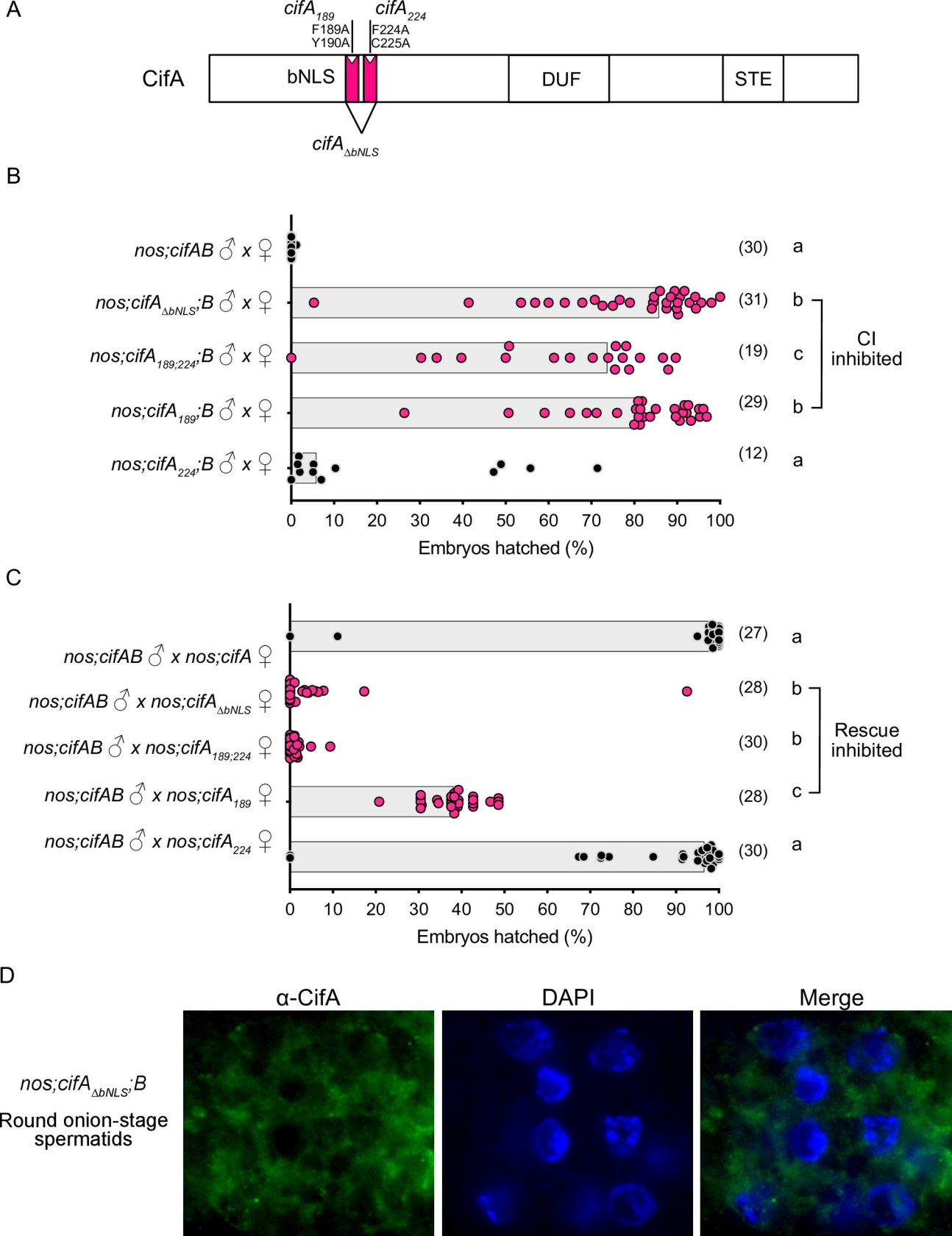
A
cifA189
F189A
Y190A
cifA224
F224A
C225A
CifA
bNLS
DUF
STE
cifAΔbNLS
B
nos;cifAB ♂ x ♀
nos;cifAΔbNLS;B ♂ x ♀
nos;cifA189;224;B ♂ x ♀
nos;cifA189;B ♂ x ♀
nos;cifA224;B ♂ x ♀
(30) a
(31) b
(19) c
(29) b
(12) a
CI inhibited
0 10 20 30 40 50 60 70 80 90 100
Embryos hatched (%)
C
nos;cifAB ♂ x nos;cifA ♀
nos;cifAB ♂ x nos;cifAΔbNLS ♀
nos;cifAB ♂ x nos;cifA189;224 ♀
nos;cifAB ♂ x nos;cifA189 ♀
nos;cifAB ♂ x nos;cifA224 ♀
(27) a
(28) b
(30) b
(28) c
(30) a
Rescue inhibited
0 10 20 30 40 50 60 70 80 90 100
Embryos hatched (%)
D
α-CifA
DAPI
Merge
nos;cifAΔbNLS;B
Round onion-stage spermatids